


Whey protein/pectin-coated W/O/W emulsion as stable vehicles for co-loading phenolic compounds of *Carya cathayensis* Sarg. peels: encapsulation and molecular dynamic behavior

Xizhe Fu^{1,2#}, Yinglin Du^{1**}, Gongnian Xiao³, Qiaojun Jia⁴, Tarun Belwal⁵, Zisheng Luo², Tianhua Huang⁶, Xiangzheng Yang⁷, Da Wang⁷, Maoyu Wu⁷ and Yanqun Xu^{2*} 

¹ Key Laboratory of Agricultural Product Processing and Quality Control of Specialty (Co-construction by Ministry and Province), School of Food Science and Technology, Shihezi University, Shihezi, Xinjiang 832000, PR China

² College of Biosystems Engineering and Food Science, Key Laboratory of Agro-Products Postharvest Handling of Ministry of Agriculture and Rural Affairs, Zhejiang University, Hangzhou, Zhejiang 310058, PR China

³ School of Biological and Chemical Engineering, Zhejiang University of Science and Technology, Hangzhou, Zhejiang 810023, PR China

⁴ College of Life Sciences and Medicine, Zhejiang Sci-Tech University, Hangzhou, Zhejiang 310018, PR China

⁵ Vegetable and Fruit Improvement Center, Texas A&M AgriLife Research, Texas A&M University, Texas, College Station, TX 77845, USA

⁶ China International Marine Containers Group, Shenzhen, Guangdong 518067, PR China

⁷ Jinan Fruit Research Institute, All China Federation of Supply and Marketing Cooperatives, Jinan, Shandong 250014, PR China

[#] Authors contributed equally: Xizhe Fu, Yinglin Du

^{*} Corresponding authors, E-mail: yinglindu@163.com; xuyanqun@zju.edu.cn

Abstract

In the present work, the whey protein/pectin complex was applied to construct a stable multiphase W/O/W emulsion to co-encapsulate phenolic compounds from *Carya cathayensis* Sarg. peels. The ratio of whey protein/pectin for the complex was optimized for better encapsulation efficiency and emulsion stability, and the ratio influence on complex structure, interface adsorption behavior, rheological properties of coated emulsion, and dynamic behavior of phenolics in inner water phase was also investigated. Results revealed that whey protein/pectin complex (at a ratio of 1:3) could form stronger gel-like network structures accounting for the highest absorption stability at the emulsion interface and larger initial particle size. The coated emulsion exhibited relatively higher viscosity, the highest storage stability, and encapsulation stability under heating process, with the highest encapsulation ratio of 93.1%. Furthermore, molecular dynamic behaviors and interactions of mainly phenolics from *Carya cathayensis* Sarg. peels in the inner water phase of emulsions were visualized and analyzed.

Citation: Fu X, Du Y, Xiao G, Jia Q, Belwal T, et al. 2025. Whey protein/pectin-coated W/O/W emulsion as stable vehicles for co-loading phenolic compounds of *Carya cathayensis* Sarg. peels: encapsulation and molecular dynamic behavior. *Food Innovation and Advances* 4(2): 201–211 <https://doi.org/10.48130/fia-0025-0019>

Introduction

Carya cathayensis Sarg. peels (CCSPs) contain various bioactive compounds, such as polyphenolics, flavonoids, naphthoquinone, polysaccharides, etc., which could account for its wide application in traditional Chinese folk medicine for hundreds of years for the treatment of rheumatic arthritis, constipation, gynaecological disorders, relieving pain, and other ailments^[1,2]. Amongst all the phytochemicals of plants, phenolic compounds are one primary class of secondary metabolites. The phenolic compounds have been paid increasing attention due to a wide variety of bioactivities such as antibacterial, antioxidant, anti-obesity, alleviation of type 2 diabetes, and other metabolic problems^[3–5]. Therefore, phenolic compounds have been widely accepted as important sources of natural food additives, preservatives, dietary supplements, and functional factors in functional food^[6–8]. In our previous work, it was revealed that the phenolic compounds of CCSPs mainly include phenolic acids, flavonols, flavanones, flavan-3-ols, etc., and 15 phenolic compounds were analyzed quantitatively, positively contributing to various antioxidation activities and inhibitory activities of glucose/starch digestion enzymes, which could be related to multiple antioxidation and potential for treatment of type 2 diabetes^[2,9].

Previous studies have shown that the encapsulation of phenolic compounds by food-grade emulsion could protect the phenolics

that are susceptible to extreme conditions^[10–12]. Emulsions as carriers for phenolics could enhance the bioavailability and biological accessibility of embedded polyphenols by slow release^[13,14], and could also serve as additives to improve the sensory properties and nutritional quality of food^[15,16]. Multi-phase W/O/W emulsion, which combine water in oil (W/O) and oil in water (O/W) emulsions, is a kind of kinetically stable system, and the amphipathic agent at the outer oil/water interface is critical to keep the W/O/W emulsion stable^[17]. Therefore, suitable food grade biomacromolecules can be selected and adjusted to the appropriate proportions to make emulsions possess ideal sensory, nutritional, processing, and other characteristics and stability^[18,19]. Compared with food-grade proteins or polysaccharides alone, protein-polysaccharide complexes can generally exhibit better-emulsifying characteristics due to their better colloidal chemical properties^[11,15,20]. Multiphase emulsions with complexes of protein-polysaccharides could serve as good carriers and protection of unstable compounds, and researchers also revealed many other ideal characteristics such as controlled release and biological accessibility improvement of the embedded bioactive compounds, natural macromolecules from food sources possessing good safety and nutritional properties. Whey protein (BWP), composed of α -lactalbumin and β -lactoglobulin, has been widely used to prepare food-grade protein-polysaccharide complexes^[21,22]. Pectin (PEC) is a natural food-grade polysaccharide

with good hydrogel characteristics, which is linked by galacturonic acid units via α -1,4 glycosidic bonds and has complex anionic groups, and high methoxy pectin has ideal hydrogel characteristics because of its higher degree of esterification, which has been utilized in the current study^[23,24]. Due to the diversity and complexity of embedded compounds, it is indispensable to construct customized W/O/W emulsions with specific compositions and ratios of protein-polysaccharide. Furthermore, the dynamic behavior processes and the interaction of embedded phenolics in the inner water phase of emulsions is not available in the current literature, demanding further investigation for potential future applications.

In this work, a multiphase W/O/W emulsion based on the whey protein-pectin (BWP-PEC) complex was constructed, and the protein-polysaccharide ratio was optimized for encapsulation of polyphenol extract of CCSPs to screen a food-grade emulsion system with higher stability (lower speed of emulsion stratification). The physico-chemical properties of multiphase W/O/W emulsion and the influence of the BWP-PEC complex on the stability of emulsions were investigated in various aspects. The dynamic behavior and interaction of phenolic compounds from CCSPs in the inner water phase of W/O/W emulsions were explored by molecular dynamic simulation to provide new insights into the mechanism of different phenolic molecule behavior in the inner water phase of W/O/W emulsions. It is anticipated that the current study can provide a stable carrier for co-loading phenolic compounds of CCSPs, and reveal the possible mechanisms of molecular behavior of embedded phenolics in the inner water phase by more specific intermolecular interaction.

Materials and methods

Materials and chemicals

Carya cathayensis Sarg. peels (CCSPs, moisture content 52.6% (w/w), fiber content 30.9% (w/w), ash content 0.7% (w/w)) were collected from a local farm market of Xihu district (Hangzhou, China). The peels were washed with ultra-pure water, dried at 35 °C for 24 h with airflow, ground into powder (40 mesh sieves) with an ultrafine grinder, and stored at 4 °C until extraction.

The whey protein (BWP, whey protein content $\geq 80\%$), propane-1,2-diol, fast green, Folin-Ciocalteu reagent, polyglycerol polyricinoleate (PGPR) were all analytical grade and purchased from Macklin Reagent Co., Ltd. (Shanghai, China). Pectin (PEC, galacturonic acid (dry base) $\geq 74\%$), Nile red were obtained from Aladdin Chemistry Co., Ltd. (Shanghai, China). Soybean oil (food grade) was bought from Yihai Kerry Co., Ltd. (Shanghai, China). Ultra-pure water was used throughout the experiment.

Extraction and determination of phenolic compounds

Ultrasound assisted extraction (UAE) of phenolic compounds from CCSPs was carried out according to a previous study with some modifications^[2]. Briefly, an ultrasonic probe (6 mm of diameter, Scientz-IIID, Ningbo Scientz Biotechnology Co., Ltd, China) was used for extraction with the following parameters: 20 kHz of ultrasonic frequency, 65 °C of extraction temperature, 10 min of ultrasonic time, 40 mL/g of solvent to solid ratio, 400 W of ultrasonic power. Ultra-pure water was utilized for extraction solvent. After extraction, the resultant mixture was centrifuged (5810R, Eppendorf AG, Germany) at 15,000 rpm for 15 min at 4 °C, and the supernatant was collected and stored at 4 °C for further experiment.

Total phenolic content (TPC) was determined based on the method previously reported with slight modification^[9]. In brief, 100 μ L sample was mixed with 500 μ L 10-fold diluted Folin-Ciocalteu reagent, and then the mixture was combined with 500 μ L Na_2CO_3 solution (7.5%, w/w) and kept in the dark at room temperature (24 °C) for 60 min. The resultant solution was measured at 765 nm, and the corresponding blank was subtracted.

Preparation of the BWP-PEC complex

The BWP-PEC complex was prepared based on a previous method with slight modifications^[25]. Briefly, BWP was dissolved in water and kept at 50 °C with magnetic stirring (RH digital, IKA Co., Ltd, Germany) for 30 min to obtain a BWP stock solution (4%, w/w). Similarly, PEC stock solution (4%, w/w) was prepared by mixing PEC and water at 50 °C with magnetic stirring for 4 h. BWP-PEC complex was prepared by mixing the corresponding stock solution at different volume ratios (BWP:PEC = 5:1, 3:1, 1:1, 1:3, 1:5, v:v) with magnetic stirring and heating at 50 °C for 3 h, and the total biopolymer concentration was kept at 4% (w/w) for all complex solutions with different volume ratios^[26,27]. The final mixture was kept at 4 °C for 12 h to complete the hydration of biopolymers.

Fourier transform infrared spectra (FTIR) analysis

The structural changes of BWP and BWP-PEC complex samples with different ratios were characterized by measuring FTIR (Nicolet iS50 Spectrometer, Thermo Scientific, Germany). All samples were freeze-dried and embedded in KBr pellets and scans were performed in wave number range of 4,000–400 cm^{-1} with a resolution of 4 cm^{-1} at an ambient temperature (25 °C).

Formulation of BWP-PEC complex coating W/O/W emulsions

The BWP-PEC complex coating W/O/W emulsions were fabricated based on a previous report with modification^[28]. In brief, the CCSPs extract solution was the inner water phase, meanwhile the oil phase (soybean oil) contained 8% PGPR (v/v). Both inner water phase and oil phase were magnetically stirred at 50 °C for 10 min, and the basic W/O emulsion was fabricated by dropwise adding 10 mL of inner water phase into 30 mL of oil phase, and stirring at 800 rpm (55 °C) for 10 min. The resultant mixture was homogenized with an ultrasonic probe (6 mm of diameter, Scientz-IIID, Ningbo Scientz Biotechnology Co., Ltd, China) with working parameters of 80 W, 55 °C, 25 kHz, 3 min, 1 s ON and 1 s OFF, and stored at 4 °C for 30 min to obtain the basic W/O emulsion. Then, 10 mL of basic W/O emulsion was similarly dropwise added into 30 mL of outer phase containing BWP or BWP-PEC complex with varying BWP:PEC ratio as mentioned previously. The mixture was magnetically stirred at 800 rpm (55 °C) for 10 min and ultrasonicated for 3 min at 55 °C with the above-mentioned working parameters to produce the final W/O/W emulsions (Fig. 1a), which were stored at 4 °C for further experiments.

Confocal laser scanning microscopy (CLSM) analysis

The microstructure of W/O/W emulsion was observed by confocal laser scanning microscopy (TCSSP8, Leica Microsystems, Germany) based on the reported methods with slight modification^[29]. Thirty μ L 100-fold diluted W/O/W emulsion was loaded on glass slides with coverslips for optical microscopy observation. For CLSM, 50 μ L mixed dye (0.1% Nile red (w/w, in propanediol) and 0.1% Fast green (w/w, in water) with a volume ratio of 1:1) was added in 500 μ L 100-fold diluted W/O/W emulsion and kept at 25 °C for 30 min to stain the protein and lipid. Then, 30 μ L of stained emulsion sample was loaded on glass slides with coverslips for CLSM observation. Fast green was excited at a wavelength of 633 nm and detected within a range of 640–700 nm. Nile red was excited at 561 nm and detected within a range of 570–620 nm.

Differential scanning calorimetry (DSC)

The thermal properties of the W/O/W emulsion were characterized by a differential scanning calorimeter (DSC30, Mettler-Toledo, Switzerland). Forty mg of emulsion was loaded into a crucible with a cover and placed in the calorimeter. The measurement was carried out from –40 to 100 °C at a rate of 5 °C/min under a nitrogen atmosphere.

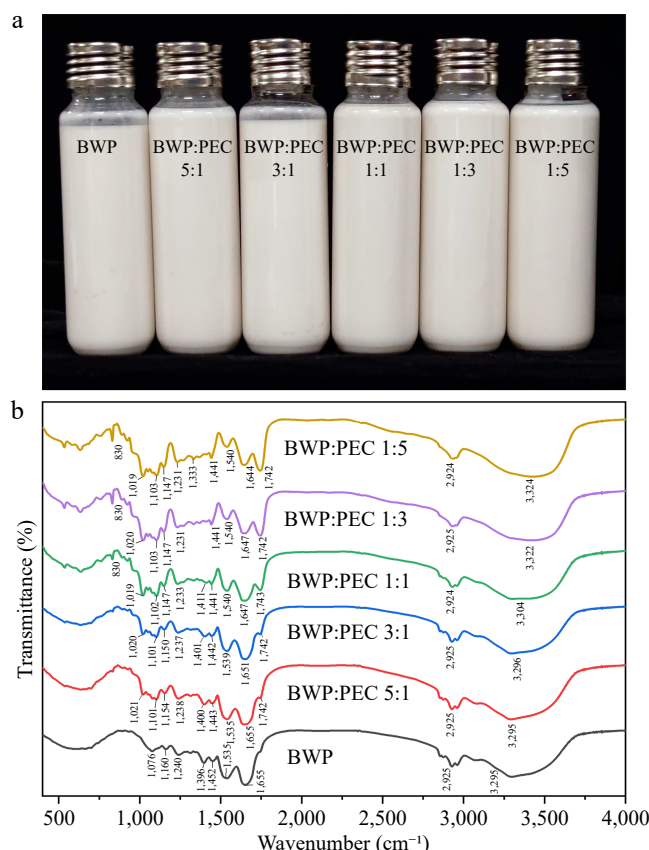


Fig. 1 Visual appearance of W/O/W emulsion at day 0 and the corresponding FTIR spectra of BWP and BWP-PEC complexes.

Adsorption stability

The adsorption stability of BWP or the BWP-PEC complex on the surface of the W/O/W emulsion was evaluated by centrifugal protocol as described elsewhere with some modification^[30]. Briefly, all the emulsions were centrifuged under 2,000, 4,000, 6,000, 8,000, 10,000 rpm at 4 °C for 15 min, respectively. The supernatant was collected and diluted 150 times and then the absorbance (*A*) was measured at 600 nm using a UV-vis spectrophotometer (UV-2550, Shimadzu, Japan). The absorbance of the corresponding initial emulsion was also measured (*A*₀), and the desorption rate was calculated as the following equation:

$$\text{Desorption rate (\%)} = (A/A_0) \times 100\% \quad (1)$$

Rheological behavior analysis

The rheological properties were measured using a rotational rheometer (MCR302, Anton Paar, Austria) based on reported work with some modifications^[31]. The measurement system was composed of two concentric parallel circle plates with a 1 mm gap and a thermostatic circulation system for temperature maintenance of samples during measuring. 0.7 mL emulsion sample was added into the gap, and the shear rate varied from 0.1 to 100 s⁻¹ at 25 °C for viscosity measurement. For the frequency sweep, a static strain of 0.1% (within the linear viscoelastic region) was set with an angular frequency ranging from 0.1 to 100 rad/s at 25 °C, and the storage modulus (*G'*) and loss modulus (*G''*) were recorded.

Encapsulation efficiency

The emulsion was centrifuged at 15,000 rpm (4 °C) for 15 min and the supernatant was collected. Similarly, a blank emulsion containing ultrapure water as inner water phase served as a reference, and the TPC was measured according to the methods above. Encapsulation

efficiency was calculated as follows:

$$\text{Encapsulation efficiency (\%)} = [1 - (A_0/A_t)] \times 100\% \quad (2)$$

where, *A*₀ was the amount of TPC added into the emulsion, and *A*_t was the amount of TPC measured in the separated supernatant phase.

Particle size and zeta potential

Particle size and zeta potential of the W/O/W emulsion was measured using a dynamic light scattering analyzer (Zetasizer Nano ZS90, Malvern Instruments Ltd., UK) according to a previous work with slight modifications^[12]. All emulsion samples were diluted 100 times with ultrapure water to eliminate multiple scatter. One mL diluted emulsion was loaded into a sample cell, and working parameters were a wavelength of 633 nm, detector angle of 90° for particle size analysis, while a voltage of 150 V for zeta potential measurement was used. All the samples were measured 20 times and the average values calculated and recorded.

Turbiscan stability analysis

The destabilization process of the emulsion was real-time evaluated and recorded by a Turbiscan analyzer (Lab Expert, Formulaction, France), which was worked out based on the static multiple-light scattering and the dispersion was measured via transmitted light and back-scattered light detectors^[32]. Eighteen mL emulsion was loaded into glass sample bottles, kept at 25 °C, and scanned every 30 min for 24 h. The Turbiscan stability index (TSI) was calculated by the corresponding Turbiscan software based on the following equation:

$$\text{TSI} = \sum_i \frac{\sum_h |\text{Scan}_i(h) - \text{Scan}_{i-1}(h)|}{H} \quad (3)$$

where, *i* represented scan numbers changed from 1 to *n*, *Scan*_{*i*}(*h*) and *Scan*_{*i-1*}(*h*) were the *i* scan and *i-1* scan at specific height *h*, and *H* indicated the height from the bottom to the meniscus of emulsion.

Stability of emulsion at high temperature

The stability for the encapsulation ratio of different emulsions under high temperature (90 °C) were evaluated. All the emulsion samples were sealed and stored under 90 °C^[28], and collected at 0, 2, 4, and 6 h. Encapsulation ratio was measured according to a previous method.

Molecular dynamic simulation analysis

Molecular dynamic simulation was performed with GROMACS 2019.6 package using Amber (99SB-ildn) force field^[33] as recently described elsewhere with slight modification^[2]. The structure of molecules, including procyanidin B1, 2,3-dihydroxybenzoic acid, pinocembrin, and procyanidin B3 were generated in Chem3D and optimized using density functional theory (DFT) under B3LYP/6-311G** level. Topology information was generated using the ANTECHAMBER module of the AmberTools package. Restrained electrostatic potential (RESP) charge was involved and calculated by Multiwfn^[34].

Procyanidin B1, 2,3-dihydroxybenzoic acid, pinocembrin, and procyanidin B3 dissolved in water were generated by Packmol (<http://leandro.iqm.unicamp.br/m3g/packmol/home.shtml>) in cube boxes of 12 nm × 12 nm × 12 nm, respectively^[35,36]. Each box consists of 40 phenolic compound molecules (Procyanidin B1/2,3-dihydroxybenzoic acid/pinocembrin/procyanidin B3) and 9988 water molecules. To facilitate the observation of molecular moving behavior, the system temperature was set at 338.15 K to accelerate the molecular motion, and 100 ns of simulation with a step value of 2 fs was performed. Other parameters and processes were the same as recorded in previous work^[2]. Moreover, Multiwfn was adopted to analyze the average noncovalent interaction (aNCI) based on the

reduced density gradient (RDG) method^[37]. The corresponding thermal fluctuation index (TFI) analysis was also carried out with Multiwfn^[34].

Statistical analysis

Statistical analysis was conducted with SPSS software (24, IBM, USA), and results were reported as means \pm standard deviation (SD). One-way analysis of variance (ANOVA) was applied with Duncan's test, which was considered statistically significantly different at $p < 0.05$.

Result and discussion

FTIR analysis of the BWP-PEC complex

FTIR was performed to evaluate the influence of interactions of macromolecule polymers on the structure of the BWP or BWP-PEC complex. As depicted in Fig. 1b, the broad band around $3,400\text{ cm}^{-1}$ represent stretching vibration of O-H groups, while specific peaks around $3,295$, $2,925$, $1,655$, and $1,535\text{ cm}^{-1}$ depicted the stretching vibration of N-H, C-H of saturated CH_2 and CH_3 , C=O of amide I and amide II, respectively^[25,38]. Peaks at $1,452$ and $1,076\text{ cm}^{-1}$ were referent to the bending vibration of C-H and C-N^[25]. With the increasing of PEC ratio in the BWP-PEC complex, the broad band around $3,400\text{ cm}^{-1}$ shifted towards the higher wavenumber, meanwhile the specific peak at $3,295\text{ cm}^{-1}$ gradually weakened, which might indicate formation of hydrogen bonds between BWP and PEC influencing the original stretching vibration of O-H and N-H^[39]. Besides, the specific peaks in BWP at $1,655$ and $1,535\text{ cm}^{-1}$ gradually shifted to $1,644$ and $1,540\text{ cm}^{-1}$ with increasing ratio of PEC, which might be attributed to newly formed hydrogen bonds and other interaction influenced the stretching vibration of C=O in amide I and amide II^[25]. Furthermore, as the PEC ratio increased in the complex, peak intensity around $1,742\text{ cm}^{-1}$ enhanced, which might be related to the increased amount of C=O groups from PEC; another enhanced peak near $1,019\text{ cm}^{-1}$ might reflect C-O-C of either group in the saccharide structure from PEC^[38]. The peak around $1,396\text{ cm}^{-1}$ decreased as the PEC ratio increased suggesting that the $-\text{COO}-$ group was influenced, possibly due to the formation of complexes changing the original structure of the group, while newly formed peaks around $1,101$ – $1,103\text{ cm}^{-1}$ might represent glucosidic bonds or other new characteristic signals during the formation of BWP-PEC complexes^[18,23].

Thermal characteristic analysis

Thermal analysis could determine the thermal properties of the emulsion, which could, to some extent, suggest structural properties. Supplementary Fig. S1 depicts the DSC plot of the W/O/W emulsion coated by the BWP or the BWP-PEC complex under temperature variations from -40 to $100\text{ }^\circ\text{C}$. It could be observed that no freezing peak appeared from -40 to $0\text{ }^\circ\text{C}$, and all the emulsions possessed only one major endothermic peak within the range of 6.23 – $10.62\text{ }^\circ\text{C}$ during the heating process, which reflected the melting of the aqueous phase^[40], meanwhile suggesting that the oil phase did not crystallize and the emulsion remained stable during the heating process from -40 to $100\text{ }^\circ\text{C}$ ^[28,41].

Storage stability of the emulsion

Table 1 shows the particle (droplet) size and zeta potential changes of coated emulsions before and after 16 d of storage at ambient temperature. Generally, as the PEC ratio increased in the BWP-PEC complex, the newly prepared emulsion (0 d) possessed bigger particle sizes, which could possibly be attributed to enhanced viscosity of the complex derived from the higher PEC ratio, thus generating a thicker coating layer and gel-like network

Table 1. Particle size and zeta potential of W/O/W emulsion at day 0 and 16.

Emulsion	Particle size (nm)		Zeta potential (mV)	
	Day 0	Day 16	Day 0	Day 16
BWP	$740.76 \pm 22.53^{\text{cB}}$	$904.40 \pm 26.24^{\text{cA}}$	$-55.03 \pm 0.59^{\text{dB}}$	$-22.30 \pm 0.46^{\text{aA}}$
BWP:PEC 5:1	$739.13 \pm 24.06^{\text{cB}}$	$1016.20 \pm 24.74^{\text{cA}}$	$-41.90 \pm 0.82^{\text{cB}}$	$-28.27 \pm 0.29^{\text{bA}}$
BWP:PEC 3:1	$798.86 \pm 26.58^{\text{cB}}$	$967.07 \pm 87.65^{\text{cA}}$	$-42.73 \pm 1.32^{\text{cB}}$	$-32.20 \pm 0.26^{\text{cA}}$
BWP:PEC 1:1	$1016.30 \pm 43.35^{\text{bB}}$	$1176.00 \pm 68.11^{\text{bA}}$	$-38.50 \pm 0.96^{\text{bB}}$	$-34.70 \pm 0.46^{\text{dA}}$
BWP:PEC 1:3	$1074.67 \pm 28.57^{\text{bA}}$	$1153.33 \pm 40.87^{\text{bA}}$	$-37.90 \pm 0.35^{\text{bA}}$	$-36.37 \pm 1.38^{\text{eA}}$
BWP:PEC 1:5	$1357.00 \pm 23.43^{\text{aB}}$	$1524.00 \pm 97.02^{\text{aA}}$	$-35.40 \pm 0.17^{\text{aB}}$	$-33.33 \pm 0.12^{\text{cA}}$

Values are shown as mean \pm standard error (n = 3); different lowercase letters in the same column represent significant difference in the column direction ($p < 0.05$); different capital letters in the same row within 'particle size' or 'zeta potential' group represent significant difference between the corresponding data of Day 0 and Day 16 ($p < 0.05$).

structure. After 16 d of storage, the particle size of each emulsion increased to a different extent: the average particle size of each emulsion coated by different macromolecules (BWP and complex with BWP:PEC ratio of 5:1, 3:1, 1:1, 1:3, 1:5) increased by 163.64 nm (22.09%), 277.07 nm (37.49%), 168.21 nm (21.06%), 159.70 nm (15.71%), 78.66 nm (7.32%), 167.00 nm (12.30%), respectively. It could be observed that the emulsion coated by the complex at BWP:PEC = 1:3 showed the lowest increasing percentage of particle size, which obviously maintained the stability of droplet size in the emulsion system. This result might be related to its excellent coating effect and relatively higher system viscosity.

Zeta potential analysis (Table 1) showed that all the newly prepared emulsion (0 d) possessed negative zeta potential (absolute value higher than 15 mV), demonstrating all the newly prepared emulsion systems possessed short-term stability. After 16 d storage, negative zeta potential values also were obtained for all tested emulsions. However, compared with the emulsions at 0 d, zeta potential values increased to different extent: zeta potential of emulsions coated by different macromolecules (BWP and complex with BWP:PEC ratio of 5:1, 3:1, 1:1, 1:3, 1:5) enhanced by 32.72 (59.48%), 13.63 (32.53%), 10.53 (24.64%), 3.80 (9.87%), 1.53 (4.04%), 2.07 (5.85%). Similar to the results in particle size analysis, the lowest enhancement ratio of zeta potential appeared in emulsions coated by the complex at 1:3 of BWP:PEC ratio, reflecting its better stability of keeping zeta potential at the emulsion interface.

Turbiscan stability analysis

Turbiscan was performed to obtain the dynamic process of emulsion stability during 24 h storage by recording backscattering spectra at specific time interval. The intensity of backscattering depends on the volume of dispersed phase and droplet size at specific height, thus characterizing the real-time emulsion stability by measuring light dispersion^[42]. As shown in Fig. 2, the backscattering intensity at the bottom layer (0–8 mm) and meniscus of emulsion (36–44 mm) exhibited obvious changes during 24 h storage of emulsions. It could be observed that the backscattering spectra at the bottom layer gradually decreased with extension of storage time, indicating that the light transmittance of bottom liquid layer increased and gradually formed relatively clear transparent water phase under the effect of gravity migration and density difference amongst various phases^[32]. Meanwhile, the top part of the emulsion rose, suggesting the droplets of emulsions coated by the BWP or BWP-PEC complex floated up driven by the density difference of the emulsion droplets in the surrounding continuous phase, and

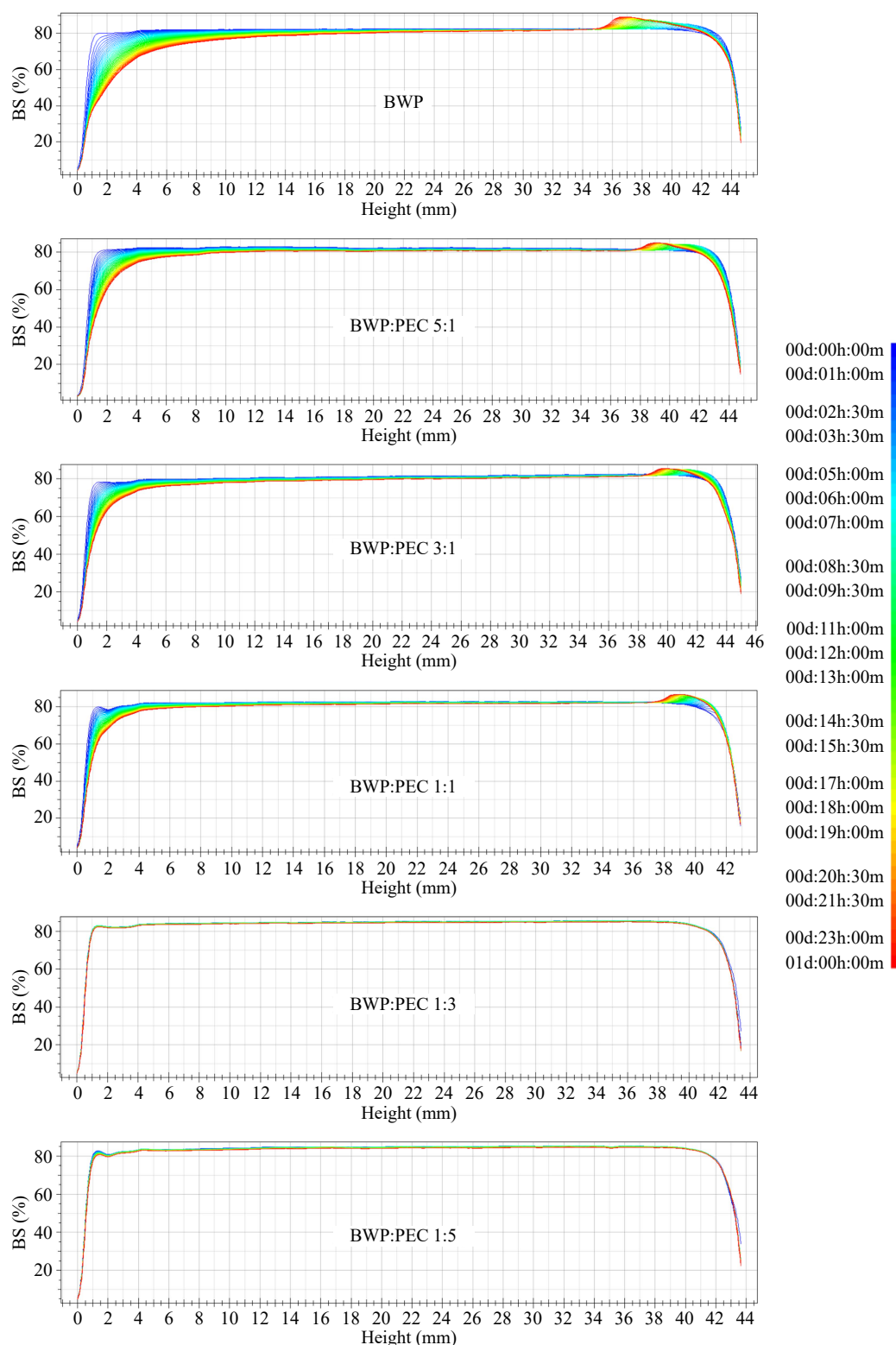


Fig. 2 Backscattering of W/O/W emulsion coated with BWP and BWP-PEC over 24 h.

gradually gathered at the top forming a paste-like layer^[43]. By comparison, a relatively higher PEC ratio in the BWP-PEC complex could result in a less descending range of backscattering intensity at the bottom layer of the emulsion, and less increasing range at the top of the emulsion layer, suggestion a relatively higher PEC ratio (BWP:PEC = 1:3 and 1:5) in the complex could affiliate to maintain the emulsion stability at the bottom and top layers.

TSI (Turbiscan stability index) value represented the changes of emulsion droplet size distribution at different heights. As shown in [Supplementary Fig. S2](#), the TSI value for each emulsion increased to different extents as the storage time extended. The TSI of emulsion coated by BWP increased dramatically higher than that of the BWP-PEC complex with longer storage time, reflecting relatively lower stability of BWP coating emulsion. By contrast, the emulsion

coated by BWP-PEC complex with a higher PEC ratio (BWP:PEC = 1:3 and 1:5) showed the slowest TSI increasing trend and lowest eventual TSI growth, demonstrating these two complexes could maintain excellent emulsion stability. Similar results were obtained by Gao et al. in their work concerning the influence of protein-chitosan complex on emulsion stability^[42].

Microstructure analysis of the W/O/W emulsion

The microstructure of the emulsion coated by BWP and BWP-PEC complex was observed by optical microscopy and CLSM. As shown in Fig. 3, it could be observed that the oil phase completely coated single or multiple co-existing inner water phases, and meanwhile was surrounded by the outer water phase (Fig. 3a–f). Different

coating materials (BWP or BWP-PEC complex) however showed differing microstructure, droplet size, and encapsulation effect.

CLSM images (Fig. 3) showed the BWP or BWP-PEC complex with green fluorescence coating the oil phase with red fluorescence, which verified the BWP or complex absorbed on the surface between the outer water phase and oil phase and formed a coating layer. Generally, the droplet size of the W/O/W emulsion coated by the BWP-PEC complex was bigger than the one coated by BWP, which might be related to stronger gel-network, and a thicker and more complete coating layer at the surface formed by the BWP-PEC complex^[20,25]. Compared with the emulsion coated with BWP, the emulsion with more compact and a thicker coating layer of the

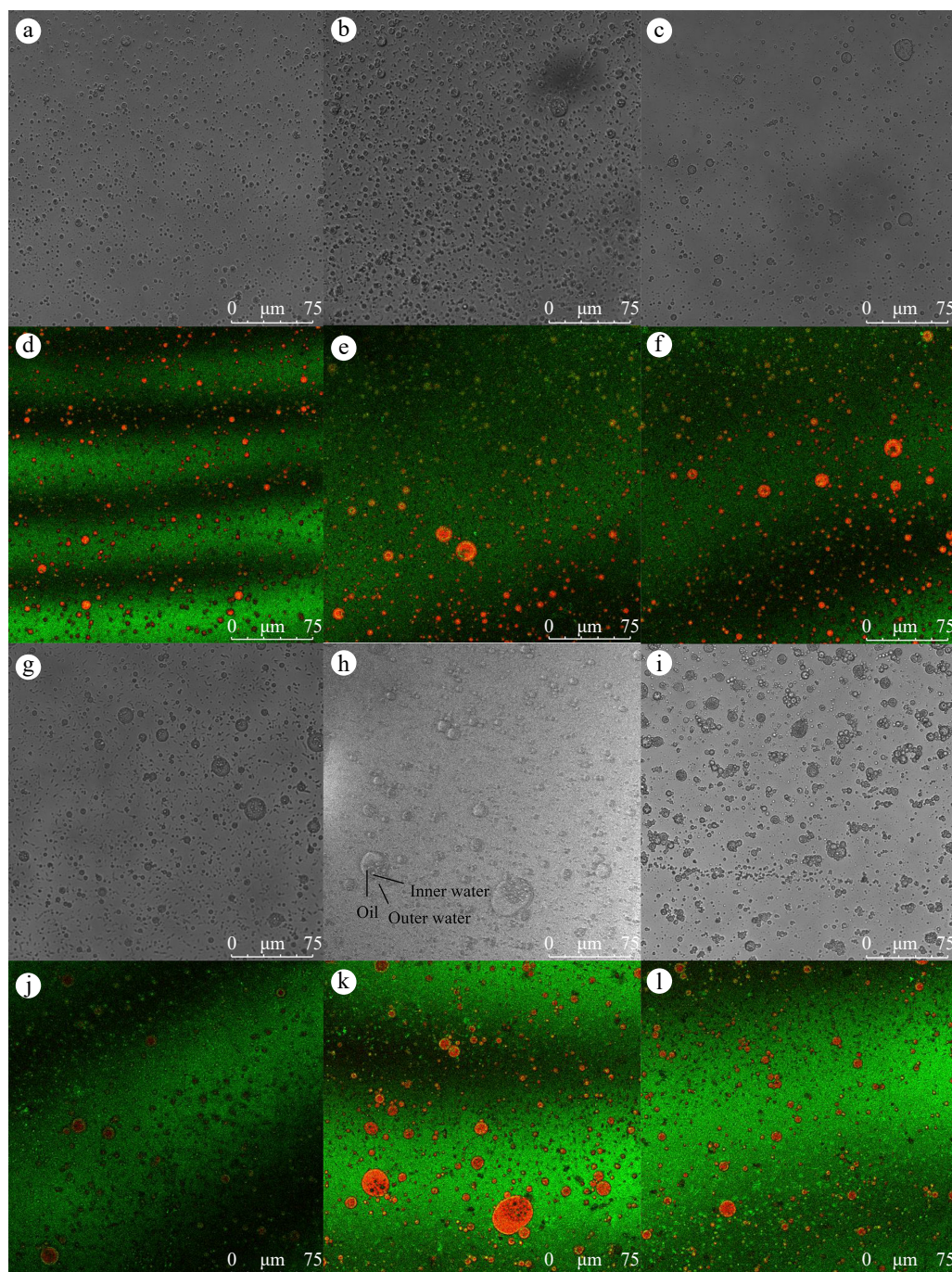


Fig. 3 Optical microscopy of W/O/W emulsion coated with (a) BWP, (b) BWP:PEC = 5:1, (c) BWP:PEC = 3:1, (g) BWP:PEC = 1:1, (h) BWP:PEC = 1:3, (i) BWP:PEC = 1:5. (d)–(f), (j)–(l) represent the corresponding (a)–(c), (g)–(i) confocal laser scanning microscopy.

BWP-PEC complex might influence the encapsulation efficiency and emulsion stability.

Absorption stability of the coated layer at the emulsion interface

To evaluate the stability of the BWP or the BWP-PEC complex absorbed at the emulsion interface between the oil phase and outer water phase, centrifugation test was performed at 2,000, 4,000, 6,000, 8,000, 10,000 rpm to distinguish adsorption capacity. Given almost no distinguishable difference of desorption ratio of BWP or the BWP-PEC complex amongst all emulsions under low-speed centrifugation (lower than 1,000 rpm), 2,000–10,000 rpm was selected to facilitate and accelerate the desorption process, and gradient increase of centrifuge speed could show the different absorption capacity of the food-grade macromolecules at emulsion interface. Under the same centrifuge speed, a lower desorption ratio suggested BWP or BWP-PEC complex possessed higher absorption stability at the emulsion interface. As shown in [Supplementary Fig. S3](#), the emulsion coated with BWP exhibited the highest desorption ratio among the tested samples, indicating the lowest absorption stability, while two BWP-PEC complexes (BWP:PEC = 1:5 and 1:3) possessed relatively lower desorption ratio at the emulsion interface, reflecting better absorption capacity. The complex of BWP:PEC = 1:3 showed the lowest desorption ratio at the emulsion interface, denoting the highest surface absorption stability.

Rheological properties of the coated emulsion

Polysaccharides are generally regarded as food thickener in the food industry, which could increase the stability, prevent delamination or precipitation^[44]. In emulsion systems, polysaccharides could also serve as stabilizers via increasing viscosity of the aqueous phase. [Figure 4a](#) depicts the viscosity of the emulsion coated by the BWP or BWP-PEC complex varied as the shear rate increased. A declining trend of viscosity for all the samples was observed with the shear rate increasing from 0.1 to 100 s⁻¹, which matches the properties of pseudo-plastic fluid^[45].

The viscosity of all emulsions dramatically decreased with the shear rate ranging from 0.1 to 10 s⁻¹, reflecting an obvious shear-thinning process. The emulsions coated by a BWP-PEC complex of BWP:PEC = 1:3 or 1:5 possess relatively higher viscosity, which was followed by a coated emulsion with a complex of BWP:PEC = 1:1. In comparison, BWP or BWP-PEC complex at a ratio of 3:1 and 5:1 coating emulsions exhibited relatively lower viscosity. It was obvious that the complex with a high ratio of PEC possessed higher viscosity, which was consistent with higher emulsion interface absorption stability of complexes with relatively higher PEC ratio, and could possibly enhance bridging flocculation effects, subsequently facilitating stability of the emulsion interface^[46,47].

To characterize stored elastic energy and dissipate viscous energy, storage modulus (G') and loss modulus (G'') of emulsions were measured by frequency sweep tests ([Fig. 4b](#)). G' values were higher than the corresponding G'' for all the samples with no crossover between G' and G'' as frequency increased, which reflected elastic behavior properties, suggesting the formation of gel-networks with similar structures with some gel properties^[46,48]. PEC showed negative change in aqueous solution, while BWP carried a positive charge below its isoelectric point. Therefore, BWP and PEC combined to form a complex by electrostatic interaction. Meanwhile, due to large numbers of methoxyl groups in PEC, electrostatic repulsion between pectin chains drove them to disperse, which facilitated the formation of a structure similar to a gel-network. As PEC ratio increased in the BWP-PEC complex, G' value of the corresponding emulsion increased ([Fig. 4b](#)). Considering a higher G' value generally indicates a stronger network structure^[22],

a higher PEC ratio in the BWP-PEC complex could affiliate to form a gel-like network structure in emulsion system, which might be attributed to more compact cross-linked structure generated from a higher ratio of PEC and BWP by electrostatic interaction. This phenomenon was also consistent with a higher PEC ratio in BWP-PEC complex assisting its absorption stability at the emulsion interface, consequently forming a more stable coating layer.

Encapsulation efficiency

The encapsulation efficiency of TPC from CCSPs is shown in [Supplementary Fig. S4](#). As the PEC ratio increased in the BWP-PEC complex, the encapsulation ratio of TPC by emulsion gradually increased, and then dramatically decreased after the ratio of BWP:PEC was 1:3, where the highest encapsulation ratio was obtained (93.1%) and significantly higher than other emulsions. Increased PEC ratio in the BWP-PEC complex could increase the viscosity and generate a stronger network structure, which may result in higher encapsulation efficiency before the BWP:PEC = 1:3. However, a higher PEC ratio (BWP:PEC = 1:5) could decrease the surface absorption stability of the BWP-PEC complex, which may lead to lower encapsulation efficiency. It could also be observed that the BWP:PEC = 1:3 forms a better W/O/W emulsion droplet structure ([Fig. 3](#)), which may also account for the best encapsulation

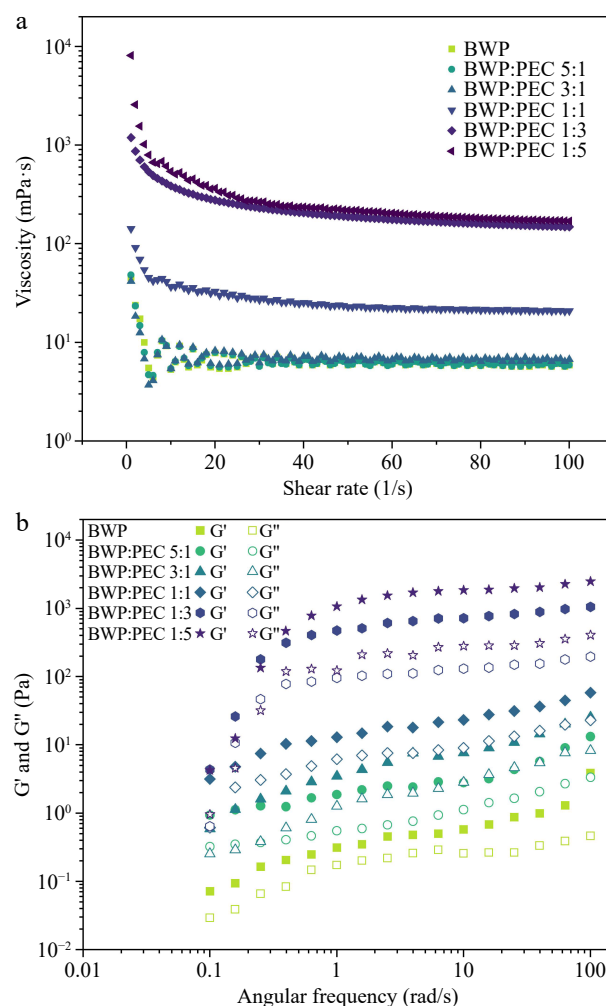


Fig. 4 (a) Viscosity vs shear rate from 0 to 100 1/s of W/O/W emulsions coated with BWP and BWP-PEC complexes. (b) Frequency sweeps curves (G' , storage modulus; G'' , loss modulus) with angular frequency from 0.1 to 100 rad/s of W/O/W emulsions coated with BWP and BWP-PEC complexes.

efficiency. Similar points were also reported by Choi & Chang, who suggested that the electrostatic interaction between protein and pectin could promote the layer formed at the emulsion interface, which might be responsible for the appropriate ratio of PEC in the BWP-PEC complex increasing the encapsulation ratio^[49]. However, it could be observed that excessive PEC increased the viscosity of the emulsion system, which might hinder the formation of gel-like network structures at the emulsion interface, thus showing negative effects on the encapsulation process.

Stability of emulsion at high temperature

Given that food processing often involves heating operations (such as sterilization, concentration, etc.), the heating processes would result in structural changes of biopolymers, which may influence their interface adsorption and encapsulation properties, and the emulsion systems were stored at 90 °C for 6 h to evaluate encapsulation stability of the emulsion under high temperature. It could be observed from [Supplementary Fig. S5](#) that the encapsulation ratio of all emulsions dramatically decreased in the first 2 h, and thereafter the general encapsulation ratio remained relatively stable as the heating time extended from 2 h to 6 h. It should be noted that the emulsion coated by BWP displayed a larger reduction of the encapsulation ratio as heating time increased continuously, while other emulsions coated by the BWP-PEC complex showed generally stability or slightly decreased the encapsulation ratio under the same heat process, which might be related to a tighter and thicker coating layer formed by the BWP-PEC complex at the emulsion interface^[49]. Besides, BWP denatured and condensed during the heating process, and prolonged heating would reduce the amount of protein adsorbed at the emulsion interface, leading to the formation of flocculent precipitate and demulsification phenomenon, which showed a negative effect on the encapsulation stability^[50]. Meanwhile, BWP and PEC in the complex might conjugate through Maillard reactions^[51,52], and affect the exposure of hydrophobic groups inside the original BWP, subsequently gradually forming tighter coating layers during heating and in turn improving the thermal stability of the emulsion^[53,54]. The emulsion coated by the complex of BWP:PEC = 1:3 possessed the highest encapsulation ratio throughout 6-h heating, indicating this ratio of complex contributed excellent encapsulation stability during heating to the coated emulsion.

Molecular dynamic simulation of phenolics dissolving in the inner water phase

The dissolution behavior of mainly phenolic compounds from CCSPs in the inner water phase of the emulsion was investigated by molecular dynamic simulation analysis, which reveals the dynamic behavior of phenolics molecules and their interaction with the inner water phase of W/O/W emulsion. As reported in our previous work^[2], procyanidin B1, 2,3-dihydroxybenzoic acid, pinocembrin, and procyanidin B3 were the main phenolic compounds in CCSPs, which were involved in the current study.

It can be seen from [Fig. 5a](#) that procyanidin B1, pinocembrin, and procyanidin B3 in the water phase exhibited a trend to form large molecular clusters from 0 to 100 ns. This phenomenon might be due to the hydrogen bond and van der Waals interaction between molecules of procyanidin B1, pinocembrin, or procyanidin B3, which drove them together to form large cluster. However, 2,3-dihydroxybenzoic acid evenly dispersed in the water phase throughout the 100 ns. This might be attributed to its relatively small molecular size with only one aromatic ring, two phenolic hydroxyl groups, and one carboxyl group, which could easily form hydrogen bonds with water molecules. Meanwhile, the hydrophobic group is relatively small, thus contributing to its even distribution in the water phase. Besides, it should be noted that 2,3-dihydroxybenzoic acid could

form multilayer structures with 2–4 molecules stacked by the aromatic ring plane in water, which might be due to the spontaneous formation of π - π stacking on the aromatic ring plane, consequently reducing the exposure of hydrophobic aromatic rings in the water phase.

Solvent accessible surface area (SASA) is a critical index that reflects the contact area between phenolic compound molecules and water molecules. From [Fig. 5b](#), SASA values of procyanidin B1, pinocembrin, and procyanidin B3 dramatically decreased in the first 10 ns and remained relatively stable and fluctuated from 10 to 100 ns. In contrast, 2,3-dihydroxybenzoic acid remained relatively stable and fluctuated throughout the 100 ns, which is consistent with the visualized dynamic behavior of phenolic compounds in [Fig. 5a](#). It should be noted that procyanidin B1 and procyanidin B3 possessed two C6-C3-C6 skeleton units (containing four aromatic rings), pinocembrin possessed one C6-C3-C6 skeleton unit (including two aromatic rings), and 2,3-dihydroxybenzoic acid had only one aromatic ring for each molecule. By comparison, as depicted in [Fig. 5c](#), the average SASA per 2,3-dihydroxybenzoic acid molecule (2.01 nm²) was slightly smaller than procyanidin B1 (2.51 nm²) and procyanidin B3 (2.81 nm²) that possessed four aromatic rings, and higher than pinocembrin (1.27 nm²) that possessed two aromatic rings, which was consistent with the large cluster formation of procyanidin B1, pinocembrin, and procyanidin B3 and even distribution of 2,3-dihydroxybenzoic acid exhibited in [Fig. 5a](#).

[Figure 5d](#) shows the quantitative description of the average hydrogen bond number per phenolic compound molecule formed with water calculated from 40 to 100 ns. The average hydrogen bond number of procyanidin B1 and procyanidin B3 formed with water phase (7.82, 7.84 hydrogen bonds, respectively) were very close and were much higher than that of 2,3-dihydroxybenzoic acid and pinocembrin with water, which were related to similar structures between procyanidin B1 and procyanidin B3, and ten hydroxyl groups and two non-hydroxyl group oxygen atoms that could serve as hydrogen bond donors or acceptors on procyanidin B1 and procyanidin B3 molecules. Despite large molecule clusters being formed by procyanidin B1 and procyanidin B3, two C6-C3-C6 skeleton units led to large space occupation for each molecule and interspace in the cluster, which allowed water molecules to pass through and form hydrogen bonds with groups inside the cluster. Meanwhile, pinocembrin possessing two hydroxyl groups and two non-hydroxyl group oxygen atoms formed fewer average hydrogen bonds than 2,3-dihydroxybenzoic acid (2.23, 2.82 hydrogen bonds, respectively). Large molecule clusters of pinocembrin might limit the exposure of hydroxyl group and non-hydroxyl group oxygen atoms to water molecules and form hydrogen bonds. Moreover, the average lifetime of hydrogen bonds shown in [Fig. 5e](#) represent the stability of the hydrogen bond in the water phase. The average lifetime of the hydrogen bond of procyanidin B1 and procyanidin B3 in water were 36.68 and 34.78 ps, which were higher than that of pinocembrin (31.28 ps) and 2,3-dihydroxybenzoic acid (25.48 ps), suggesting the hydrogen bond formed of procyanidin B1 and procyanidin B3 in the water phase were more stable than that formed of pinocembrin and 2,3-dihydroxybenzoic acid.

Given the dynamic process concerning the specific noncovalent interaction between phenolic compound molecules and water molecules, the average noncovalent interaction (aNCI) and thermal fluctuation index (TFI, indicating the stability of noncovalent interaction between phenolic compound molecules and water molecules) was performed to quantitatively characterize the different noncovalent interaction contribution, such as typical hydrogen bond, π -hydrogen bond, van der Waals interaction, steric effect, and their stability (thermal fluctuation properties)^[2]. As shown in [Supplementary Fig. S6](#), for the aNCI analysis, the red area shows the steric effect,

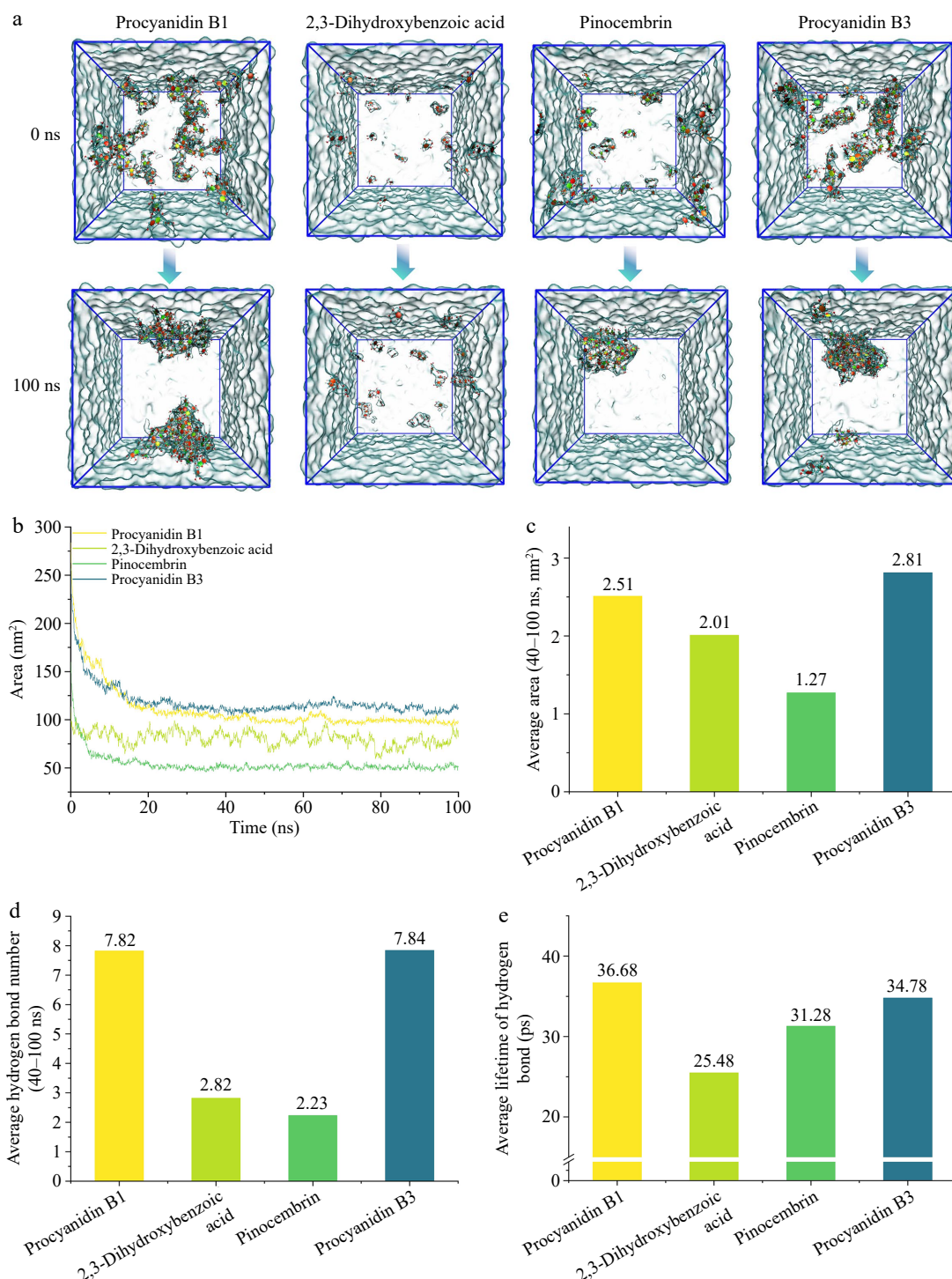


Fig. 5 Molecular dynamic simulation analysis. (a) Snapshots of procyanidin B1, 2,3-dihydroxybenzoic acid, pinocembrin, and procyanidin B3 in the water system at 0 and 100 ns, respectively. (b), (c) Solvent accessible surface area (SASA) of four of the above-mentioned phenolics in water varied from 0 to 100 ns and corresponding average SASA (per phenolic molecule) calculated from 40 to 100 ns. (d) Average hydrogen bond number (per phenolic molecule) from 40 to 100 ns. (e) Average lifetime of hydrogen bonds between the four above-mentioned phenolics and water.

which was mainly generated in the center of aromatic rings and in the vicinity of oxygen atoms. The green area surrounding the phenolic compound molecules represent van der Waals interaction, and the area color gradually changed from green to blue near the aromatic ring surface center indicating weak π -hydrogen bond interaction regions. The dark blue region near the hydroxyl groups suggests typical hydrogen bonds. It should be noted that two adjacent hydroxyl groups on an aromatic ring of phenolic compounds

could form intramolecular hydrogen bonds, which might influence the hydrogen bond formation with water molecules. TFI analysis demonstrated the stability of the noncovalent interaction displayed in a NCI analysis, and the color calibration changed from red to dark blue indicating that the interaction varied from weak to stable. From TFI analysis, it could be observed that the relatively weak interactions mainly appeared in the steric effect region near the oxygen atoms, π -hydrogen bond close to aromatic ring surface, and partial

van der Waals interaction regions surrounding phenolic compound molecules, while relatively stable interaction was basically distributed in the center of the ring structure (steric effect), and in the vicinity of the hydroxyl group (typical hydrogen bond). Similarly, Xing et al. visualized the dynamic behavior of glabridin and isoliquiritigenin in different liquid phases, and partially revealed the interaction mechanism^[55].

Conclusions

The current study showed the whey protein/pectin complex as a potential alternative to build a stable W/O/W emulsion for co-microencapsulating phenolic compounds from *Carya cathayensis* Sarg. peels. The proportion of whey protein and pectin in the complex were optimized for co-encapsulation of phenolics from *Carya cathayensis* Sarg. peels. When the ratio of whey protein and pectin reached 1:3, the whey protein/pectin complex could form a more stable gel-like network structure, possessing the highest absorption stability at the interface of the W/O/W emulsion, exhibiting the highest encapsulation efficiency, the best emulsion storage stability, and relatively high encapsulation stability under heating. Moreover, the dynamic behaviors and the interaction with water molecules of main phenolic compounds (including procyanidin B1, 2,3-dihydroxybenzoic acid, pinocembrin, and procyanidin B3) from *Carya cathayensis* Sarg. peels in the inner water phase of the emulsion were quantitatively characterized. Overall, the whey protein/pectin complex coated W/O/W emulsion could be a stable carrier for co-loading phenolic compounds from *Carya cathayensis* Sarg. peels, which provided an essential reference for further research on co-loading phenolics with different dynamic properties. Furthermore, it is necessary to investigate the application of emulsions in real food systems and its influence on food properties, which is the basis for its application in the food and cosmetics industries.

Author contributions

The authors confirm contribution to the paper as follows: study conception and design: Fu X, Xu Y, Luo Z; data collection: Du Y, Xiao G, Huang T; analysis and interpretation of results: Fu X, Jia Q, Xu Y, Yang X, Wang D, Wu M; draft manuscript preparation: Fu X, Du Y, Belwal T. All authors reviewed the results and approved the final version of the manuscript.

Data availability

All data generated or analyzed during this study are included in this published article, and its supplementary information files.

Acknowledgments

The authors would like to acknowledge the support from the Key Research and Development Program of Zhejiang Province (2023C02042), XPCC Guiding Science and Technology Plan Project (2023ZD086), Shihezi University High-Level Talents Research Initiation Project (RCZK202353), Open Project of Key Laboratory of Xinjiang Phytomedicine Resource and Utilization, Ministry of Education (XPRU202205), China.

Conflict of interest

The authors declare that they have no conflict of interest.

Supplementary information accompanies this paper at (<https://doi.org/10.48130/fia-0025-0019>)

Dates

Received 13 November 2024; Revised 24 January 2025; Accepted 18 February 2025; Published online 30 May 2025

References

1. Zhang SY, Chen AL, Li Q. 2012. Novel benzofuran constituent from the husk of *Carya cathayensis* Sarg. *Phytochemistry Letters* 5:473–75
2. Fu X, Belwal T, He Y, Xu Y, Li L, et al. 2022. UPLC-Triple-TOF/MS characterization of phenolic constituents and the influence of natural deep eutectic solvents on extraction of *Carya cathayensis* Sarg. peels: composition, extraction mechanism and in vitro biological activities. *Food Chemistry* 370:131042
3. Gowd V, Karim N, Shishir MRI, Xie L, Chen W. 2019. Dietary polyphenols to combat the metabolic diseases via altering gut microbiota. *Trends in Food Science & Technology* 93:81–93
4. Cai R, Yuan Y, Cui L, Wang Z, Yue T. 2018. Cyclodextrin-assisted extraction of phenolic compounds: current research and future prospects. *Trends in Food Science & Technology* 79:19–27
5. Ren Z, Yang H, Zhu C, Fan D, Deng J. 2023. Dietary phytochemicals: as a potential natural source for treatment of Alzheimer's disease. *Food Innovation and Advances* 2:36–43
6. Zamuz S, Munekata PES, Dzuovor CKO, Zhang W, Sant'Ana AS, et al. 2021. The role of phenolic compounds against *Listeria monocytogenes* in food. A review. *Trends in Food Science & Technology* 110:385–92
7. Guan H, Zhang W, Sun-Waterhouse D, Jiang Y, Li F, et al. 2021. Phenolic-protein interactions in foods and post ingestion: switches empowering health outcomes. *Trends in Food Science & Technology* 118:71–86
8. Roasa J, De Villa R, Mine Y, Tsao R. 2021. Phenolics of cereal, pulse and oilseed processing by-products and potential effects of solid-state fermentation on their bioaccessibility, bioavailability and health benefits: a review. *Trends in Food Science & Technology* 116:954–74
9. Fu X, Wang D, Belwal T, Xu Y, Li L, Luo Z. 2021. Sonication-synergistic natural deep eutectic solvent as a green and efficient approach for extraction of phenolic compounds from peels of *Carya cathayensis* Sarg. *Food Chemistry* 355:129577
10. Mwangi WW, Lim HP, Low LE, Tey BT, Chan ES. 2020. Food-grade Pickering emulsions for encapsulation and delivery of bioactives. *Trends in Food Science & Technology* 100:320–32
11. Cui F, Zhao S, Guan X, McClements DJ, Liu X, et al. 2021. Polysaccharide-based Pickering emulsions: formation, stabilization and applications. *Food Hydrocolloids* 119:106812
12. Zhang R, Li L, Ma C, Ettoumi FE, Javed M, et al. 2022. Shape-controlled fabrication of zein and peach gum polysaccharide based complex nanoparticles by anti-solvent precipitation for curcumin-loaded Pickering emulsion stabilization. *Sustainable Chemistry and Pharmacy* 25:100565
13. Heidari F, Jafari SM, Ziaifar AM, Malekjani N. 2022. Stability and release mechanisms of double emulsions loaded with bioactive compounds; a critical review. *Advances in Colloid and Interface Science* 299:102567
14. Pizones Ruiz-Henestrosa VM, Ribourg L, Kermarrec A, Anton M, Pilosof A, et al. 2022. Emulsifiers modulate the extent of gastric lipolysis during the dynamic in vitro digestion of submicron chia oil/water emulsions with limited impact on the final extent of intestinal lipolysis. *Food Hydrocolloids* 124:107336
15. Yan X, Ma C, Cui F, McClements DJ, Liu X, et al. 2020. Protein-stabilized Pickering emulsions: formation, stability, properties, and applications in foods. *Trends in Food Science & Technology* 103:293–303
16. Yin X, Dong H, Cheng H, Ji C, Liang L. 2022. Sodium caseinate particles with co-encapsulated resveratrol and epigallocatechin-3-gallate for inhibiting the oxidation of fish oil emulsions. *Food Hydrocolloids* 124:107308
17. Xiao Y, Ahmad T, Belwal T, Aadil RM, Siddique M, et al. 2023. A review on protein based nanocarriers for polyphenols: interaction and stabilization mechanisms. *Food Innovation and Advances* 2:193–202
18. Assadpour E, Jafari SM, Maghsoudlou Y. 2017. Evaluation of folic acid release from spray dried powder particles of pectin-whey protein nanocapsules. *International Journal of Biological Macromolecules* 95:238–47

19. Joye IJ, McClements DJ. 2014. Biopolymer-based nanoparticles and microparticles: Fabrication, characterization, and application. *Current Opinion in Colloid & Interface Science* 19:417–27
20. Ribeiro EF, Morell P, Nicoletti VR, Quiles A, Hernando I. 2021. Protein- and polysaccharide-based particles used for Pickering emulsion stabilization. *Food Hydrocolloids* 119:106839
21. Albano KM, Cavallieri ÁLF, Nicoletti VR. 2019. Electrostatic interaction between proteins and polysaccharides: Physicochemical aspects and applications in emulsion stabilization. *Food Reviews International* 35:54–89
22. Raei M, Rafe A, Shahidi F. 2018. Rheological and structural characteristics of whey protein-pectin complex coacervates. *Journal of Food Engineering* 228:25–31
23. Bettani SR, de Oliveira Ragazzo G, Leal Santos N, Kieckbusch TG, Gaspar Bastos R, et al. 2019. Sugar cane vinasse and microalgal biomass in the production of pectin particles as an alternative soil fertilizer. *Carbohydrate Polymers* 203:322–30
24. Giacomazza D, Sabatino MA, Catena A, Leone M, San Biagio PL, et al. 2014. Maltose-conjugated chitosans induce macroscopic gelation of pectin solutions at neutral pH. *Carbohydrate Polymers* 114:141–48
25. Huang H, Belwal T, Aalim H, Li L, Lin X, et al. 2019. Protein-polysaccharide complex coated W/O/W emulsion as secondary microcapsule for hydrophilic arbutin and hydrophobic coumaric acid. *Food Chemistry* 300:125171
26. Hasanvand E, Rafe A. 2018. Characterization of Flaxseed Gum/Rice Bran Protein Complex Coacervates. *Food Biophysics* 13:387–95
27. Hasanvand E, Rafe A, Emadzadeh B. 2018. Phase separation behavior of flaxseed gum and rice bran protein complex coacervates. *Food Hydrocolloids* 82:412–23
28. Huang H, Belwal T, Liu S, Duan Z, Luo Z. 2019. Novel multi-phase nano-emulsion preparation for co-loading hydrophilic arbutin and hydrophobic coumaric acid using hydrocolloids. *Food Hydrocolloids* 93:92–101
29. Aditya NP, Aditya S, Yang HJ, Kim HW, Park SO, et al. 2015. Curcumin and catechin co-loaded water-in-oil-in-water emulsion and its beverage application. *Journal of Functional Foods* 15:35–43
30. Huang GQ, Sun YT, Xiao JX, Yang J. 2012. Complex coacervation of soybean protein isolate and chitosan. *Food Chemistry* 135:534–39
31. Wu C, Li Y, Du Y, Wang L, Tong C, et al. 2019. Preparation and characterization of konjac glucomannan-based bionanocomposite film for active food packaging. *Food Hydrocolloids* 89:682–90
32. Huang H, Belwal T, Li L, Xu Y, Zou L, et al. 2021. Amphiphilic and biocompatible DNA origami-based emulsion formation and nanopore release for anti-melanogenesis therapy. *Small* 17:e2104831
33. Abraham MJ, Murtola T, Schulz R, Páll S, Smith JC, et al. 2015. GROMACS: High performance molecular simulations through multi-level parallelism from laptops to supercomputers. *SoftwareX* 1-2:19–25
34. Lu T, Chen F. 2012. Multiwfn: a multifunctional wavefunction analyzer. *Journal of Computational Chemistry* 33:580–92
35. Martínez L, Andrade R, Birgin EG, Martínez JM. 2009. PACKMOL: a package for building initial configurations for molecular dynamics simulations. *Journal of Computational Chemistry* 30:2157–64
36. Martínez JM, Martínez L. 2003. Packing optimization for automated generation of complex system's initial configurations for molecular dynamics and docking. *Journal of Computational Chemistry* 24:819–25
37. Johnson ER, Keinan S, Mori-Sánchez P, Contreras-García J, Cohen AJ, et al. 2010. Revealing Noncovalent Interactions. *Journal of the American Chemical Society* 132:6498–506
38. Albano KM, Nicoletti VR. 2018. Ultrasound impact on whey protein concentrate-pectin complexes and in the O/W emulsions with low oil soybean content stabilization. *Ultrasonics Sonochemistry* 41:562–71
39. Pirestani S, Nasirpour A, Keramat J, Desobry S, Jasniewski J. 2018. Structural properties of canola protein isolate-gum Arabic Maillard conjugate in an aqueous model system. *Food Hydrocolloids* 79:228–34
40. Zhu XF, Zhang N, Lin WF, Tang CH. 2017. Freeze-thaw stability of pickering emulsions stabilized by soy and whey protein particles. *Food Hydrocolloids* 69:173–84
41. Clause D, Lanoisellé JL, Pezron I, Saleh K. 2018. Formulation of a water-in-oil emulsion encapsulating polysaccharides to improve the efficiency of spraying of plant protection products. *Colloids and Surfaces A: Physicochemical and Engineering Aspects* 536:96–103
42. Gao S, Yang M, Luo Z, Ban Z, Pan Y, et al. 2022. Soy protein/chitosan-based microsphere as stable biocompatible vehicles of oleanolic acid: an emerging alternative enabling the quality maintenance of minimally processed produce. *Food Hydrocolloids* 124:107325
43. Saari H, Wahlgren M, Rayner M, Sjöö M, Matos M. 2019. A comparison of emulsion stability for different OSA-modified waxy maize emulsifiers: Granules, dissolved starch, and non-solvent precipitates. *PLoS One* 14:e0210690
44. Li JM, Nie SP. 2016. The functional and nutritional aspects of hydrocolloids in foods. *Food Hydrocolloids* 53:46–61
45. Gong J, Wang L, Wu J, Yuan Y, Mu R-J, et al. 2019. The rheological and physicochemical properties of a novel thermosensitive hydrogel based on konjac glucomannan/gum tragacanth. *LWT* 100:271–77
46. Wang X, Li X, Xu D, Zhu Y, Cao Y, et al. 2019. Modulation of stability, rheological properties, and microstructure of heteroaggregated emulsion: Influence of oil content. *LWT* 109:457–66
47. Lu W, Zheng B, Miao S. 2018. Improved emulsion stability and modified nutrient release by structuring O/W emulsions using konjac glucomannan. *Food Hydrocolloids* 81:120–28
48. Albano KM, Franco CML, Telis VRN. 2014. Rheological behavior of Peruvian carrot starch gels as affected by temperature and concentration. *Food Hydrocolloids* 40:30–43
49. Choi YR, Chang YH. 2018. Microencapsulation of gallic acid through the complex of whey protein concentrate-pectic polysaccharide extracted from *Ulmus davidiana*. *Food Hydrocolloids* 85:222–28
50. Setiowati AD, Wijaya W, Van der Meer P. 2020. Whey protein-polysaccharide conjugates obtained via dry heat treatment to improve the heat stability of whey protein stabilized emulsions. *Trends in Food Science & Technology* 98:150–61
51. Consoli L, Dias RAO, Rabelo RS, Furtado GF, Sussulini A, et al. 2018. Sodium caseinate-corn starch hydrolysates conjugates obtained through the Maillard reaction as stabilizing agents in resveratrol-loaded emulsions. *Food Hydrocolloids* 84:458–72
52. Meng J, Kang TT, Wang HF, Zhao BB, Lu RR. 2018. Physicochemical properties of casein-dextran nanoparticles prepared by controlled dry and wet heating. *International Journal of Biological Macromolecules* 107:2604–10
53. Wagoner TB, Foegeding EA. 2017. Whey protein-pectin soluble complexes for beverage applications. *Food Hydrocolloids* 63:130–38
54. Pirestani S, Nasirpour A, Keramat J, Desobry S, Jasniewski J. 2017. Effect of glycosylation with gum Arabic by Maillard reaction in a liquid system on the emulsifying properties of canola protein isolate. *Carbohydrate Polymers* 157:1620–27
55. Xing C, Cui WQ, Zhang Y, Zou XS, Hao JY, et al. 2022. Ultrasound-assisted deep eutectic solvents extraction of glabridin and isoliquiritigenin from *Glycyrrhiza glabra*: optimization, extraction mechanism and in vitro bioactivities. *Ultrasonics Sonochemistry* 83:105946



Copyright: © 2025 by the author(s). Published by Maximum Academic Press on behalf of China Agricultural University, Zhejiang University and Shenyang Agricultural University. This article is an open access article distributed under Creative Commons Attribution License (CC BY 4.0), visit <https://creativecommons.org/licenses/by/4.0/>.